Bulgarian Chemical Communications, Volume 50, Special Issue F (pp. 23–30) 2018

Conformational polymorphism in (3-acetamidophenyl)boronic acid

V. M. Dyulgerov*, L. T. Dimowa, R. Rusev, R. P. Nikolova, B. L. Shivachev

Institute of Mineralogy and Crystallography "Acad. Ivan Kostov", Bulgarian Academy of Sciences, Acad. G. Bonchev str., bl. 107, 1113 Sofia, Bulgaria

Received October 10, 2018; Accepted November 29, 2018

This study focuses on the structural peculiarities of two conformational polymorphs of (3-acetamidophenyl)boronic acid, $C_8H_{10}BNO_3$. The two polymorphs were generated by crystallization from different solvents: chloroform and ethanol. The crystal structures of both polymorphs have been characterized by single-crystal X-ray diffraction analyses, DTA/TG and FTIR. Single crystal analyses showed that the title compound crystallizes in the triclinic system space group $P\bar{1}$ (No 2) and in the monoclinic crystal system, space group $P2_1/c$ (No 14) in function of the employed crystallization solvent. The differences between the two crystal structures are centered on the different hydrogen bonding pattern, producing a different three-dimensional arrangement of the molecules. The DTA/TG and FTIR spectra of the two polymorphs are nearly identical and therefore they are not very suitable for differentiation. The DFT calculations showed that the energy minima of the two polymorphs differ by 0.9 kcal.mol^{-1} while the generated potential energy surface revealed a low value of 5.8 kCal mol^{-1} for the barrier of rotation of the acetamide group.

Keywords: boronic acid, conformational polymorphism, single crystal, FTIR, DTA, ab initio calculations.

INTRODUCTION

Synthetic boronic acids are widely used in organic chemistry as chemical building blocks in the Suzuki (carbon-carbon bond forming) reaction [1, 2], in medicine e.g. Boron Neutron Capture Therapy (BNCT) [3, 4] as anticancer agents [5, 6], as saccharide binders [7, 8] and as a stable synthon for crystal engeenering. Nowadays boronic acids are also investigated as potential sensors and indicators for the identification of metabolites in the disease and pathology of diabetes [9]. Boronic acids form consistent hydrogen bonds based on the $-B(OH)_2$ fragment, and these weak interactions are seemingly independent of the different substitution groups. The repeatability of the hydrogen bonding pattern is due to the formation of strong cyclic O—H...O hydrogen bonds from the $B(OH)_2$ group, analogous to the interaction of –COOH, usually producing a $R_2^2(8)$ graph set, [10, 11]. One should note that such type of hydrogen bonding interactions (e.g. $R_2^2(8)$) are amongst the most frequently encountered and employed for crystal engineering [12–14]. In solid state of materials polymorphism occurs when one chemical (with conserved composition and geometrical features) produces more than one crystalline phase [15]. However most of the organic molecules with bulky substituents linked by single bonds exhibit free rotation resulting in a huge number of possible conformations. The phenomenon, when different conformers occur in different crystal forms is termed conformational polymorphism (the chemical composition is conserved, but the geometry of the building unit is different usually) [16]. They are two other frequently discussed cases of "polymorphism": tautomerism and desmotropy. The latest generally requires a proton "relocation" [15]. The present work emphases on the structural particularities of two conformational polymorph of (3-acetamidophenyl)boronic acid based on single crystal, FTIR, DTA and DFT experiments.

MATERIALS

The (3-acetamidophenyl)boronic acid was obtained from Frontier Scientific and employed as is. The employed chloroform and ethanol were liquid chromatography grade, (LiChrosolv, Merck). Crystals of the two polymorphic conformers, suitable for single crystal X-ray diffraction analyses were grown by slow evaporation from chloroform (**1**) and ethanol (**2**).

* To whom all correspondence should be sent:
Email: silver_84@mail.bg

EXPERIMENTAL SECTION

The FTIR spectra (4000–400cm^{-1}) of compounds were recorded in KBr pellets on a Bruker, Tensor37 spectrophotometer.

The thermogravimetric (TG) and differential thermal analysis (DTA) curves in the 20–250 °C temperature range were obtained from samples of crystalized pieces (sample weight ~10 mg) placed in corundum crucibles, under a constant heating rate of 10 °C min^{-1} and argon flow of 40 ml min^{-1} on a Stanton Redcroft thermo-analyzer. The stability of the compounds and eventual phase transitions were derived from these studies.

The crystallographic analysis of **compound 1** was carried out on an EnrafNonius CAD4 diffractometer, using graphite monochromatic Mo-Kα radiation (λ = 0.7107 Å) at room temperature and $\omega/2\theta$ technique. The unit cell parameters for compound **1** were determined from 15 reflections and refined by employing 22 higher-angle reflections (17.92 < θ < 19.46°). CAD-4 Nonius Diffractometer

Table 1. Important crystallographic and refinement details for compounds **1** and **2**

Compound	**1**	**2**
Chemical formula	$C_8H_{10}BNO_3$	$C_8H_{10}BNO_3$
MW	178.98	178.98
Crystal system	Triclinic	Monoclinic
SG	P–1	$P2_1/c$
a [Å]	5.028 (3)	4.9039 (3)
b [Å]	5.055 (4)	18.1624 (9)
c [Å]	17.035 (6)	9.7928 (6)
α [°]	82.85 (2)	90
β [°]	82.70 (2)	93.911(6)
γ [°]	87.454 (9)	90
V [Å^3]	425.9 (4)	870.18(9)
Z	2	4
*F*000	188	376
Dx [Mg m^{-3}]	1.396	1.366
Radiation, λ [Å]	Mo*K*α, 0.7107	Mo*K*α, 0.7107
Cell parameters	From 22 reflections	From 1237 reflections
μ [mm^{-1}]	0.10	0.10
T [K]	290	290
Crystal size [mm^3]	0.24 × 0.21 × 0.19	0.31 × 0.25 × 0.21
Radiation source	Fine focus sealed tube	SuperNova (Mo) micro-focus X-ray source
monochromator	Graphite	Mirror
Detector	Scintillation, LiI	Atlas CCD, 10.3974 pixels mm^{-1}
Data collection x scans	non-profiled $\omega/2\theta$ scans	ω scans
Measured reflections	2480	5741
Independent reflections	2017	2904
Reflections with $I > 2\sigma(I)$	1172	1129
Parameters	122	119
R_{int}	0.035	0.039
$\theta_{max}/\theta_{min}$ [°]	28.0/1.2	32.7/3.1
h max/min	6, –6	4, –7
k max/min	6, –6	24, –27
l max/min	3, –22	14, –14
Absorption correction	none	Multi-scan
T_{min}/T_{max}	none	0.572, 1
Refinement	on F^2	on F^2
Least-squares matrix	full	full
$R[F^2 > 2\sigma(F^2)]$/all	0.0595/0.1184	0.0537/0.1497
$wR(F^2)$	0.187	0.122
S (GOF)	1.2	0.79
Hydrogen site location	Inferred from neighboring sites	Inferred from neighboring sites
(Δ/σ)max	< 0.001	< 0.001
Δρmax/Δρmin [e Å^{-3}]	0.24/–0.23	0.23/–0.25

Control Software was used for data collection [17]. The diffraction data of **compound 2** were collected at room temperature on an Agilent Diffraction SupernovaDual four-circle diffractometer equipped with Atlas CCD detector, mirror monochromatized Mo*K*α radiation from micro-focus source (λ = 0.7107 Å) using *ω*-scan technique. The determination of cell parameters, data integration, scaling and absorption correction for compound **2**, were carried out using the CrysAlisPro program package [18].

Both structures were solved by direct methods and were refined by the full-matrix least-squares method using ShelXS97 and ShelXL97 computer programs [19]. The molecular graphics were made by *ORTEP-3* for Windows [20] and crystal packing were drawn using Mercury [21]. The non-hydrogen atoms were refined anisotropically, N and O hydrogen atoms were located from difference Fourier map while carbon hydrogen atoms were placed at idealized positions. All hydrogen atoms were refined using the riding model. A summary of the fundamental crystal and refinement data is provided in Table 1. Crystallographic data (excluding structure factors) for the structural analysis were deposited with the Cambridge Crystallographic Data Centre, CCDC No. 993979 and 993980. A copy of this information may be obtained free of charge from: The Director, CCDC, 12Union Road, Cambridge, CB21EZ,UK. Fax: +441223336033, e-mail: deposit@ccdc.cam.ac.uk, or www.ccdc.cam.ac.uk.

Density functional calculations were carried out using the Gaussian 09 package [22]. Geometry optimizations employed the B3LYP/6-31+G(d) level of theory [23, 24]. Vibrational frequencies were calculated for optimized structures at the same theory level in order to confirm that the optimized structures are true stationary points.

RESULTS AND DISCUSSION

The DTA/TG curves (effects) of the two polymorphs are shown on Fig. 1. Around 145 °C both compounds exhibit an *endo* effect (related to melting). At the same temperature the TG shows ~8% weight losses, occurring a little bit slower in **1**. The overall impression from the DTA/TG experiment is to expect a similar comportment of the two crystalline forms.

The crystal structure analysis showed that compound **1** crystallizes in the triclinic system space group *P*–1 (No2) while compound **2** crystallizes in the monoclinic crystal system, space group $P2_1/c$ (No 14). In both structures (**1** and **2)** only one independent molecule is present in the asymmetric unit cell Fig. 2. The molecular features (bond

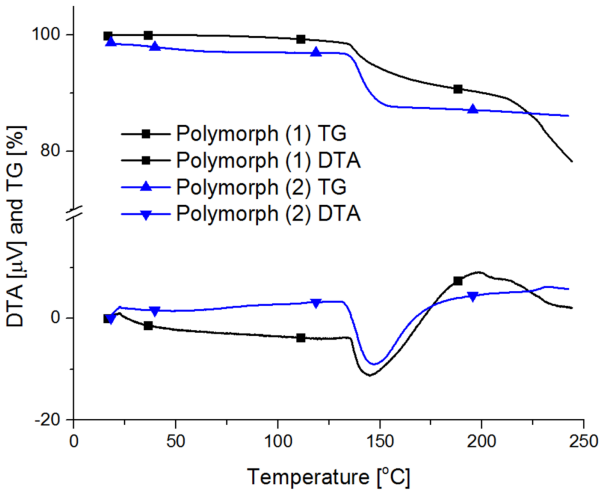

Fig. 1. DTA/TG curves for compound **1** and compound **2**.

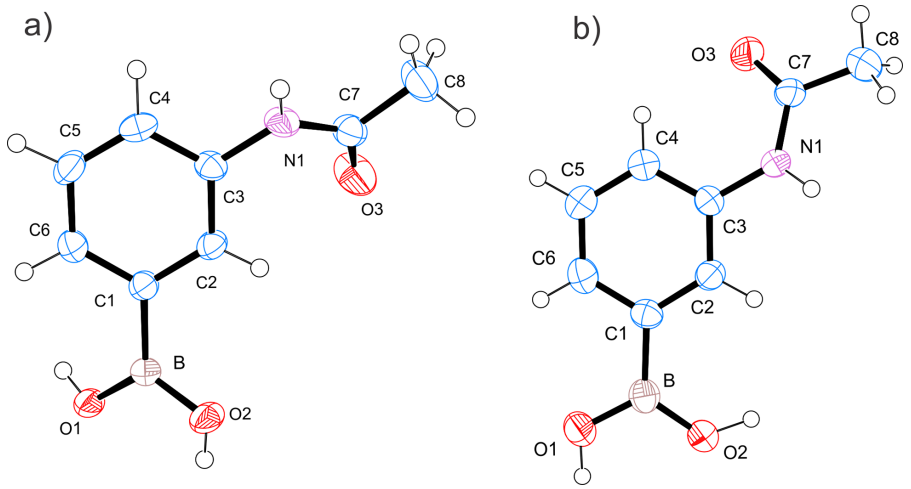

Fig. 2. *ORTEP*[20] drawings of the basic crystallographic units: *a*) **1**; *b*) **2**; ellipsoids are at 50% probability while the hydrogen atoms are shown as small spheres of arbitrary radii.

lengths and angles) of the molecules of **1** and **2** are comparable (Table 2) and are quite close to those commonly encountered in related compounds [25, 26]. For comparison, a superposition of the two independent molecules and a superposition using only the phenyl boronic moiety is presented in Fig. 3.

One can clearly see the *cis* (**1**) and *trans* (**2**) conformational isomers (or the *syn*/*anti* orientation of the carbonyl to $B(OH)_2$ group, Fig. S2). The values of the C-N-C angle (C3-N1-C7) of 126.9(2)° and 127.62(14)° in **1** and **2** respectively, are somewhat higher than 120° and thus the N atom is probably not sp^2 hybridized (the mean value for the C-N-C angle as obtained from CCDC-CSD is 122.194° see Fig. S1). In addition to the *cis*/*trans* isomerism the hydrogen atoms of O1 and O2 are in *anti*/*syn* and *syn*/*anti* positions in **1** and **2** respectively. As one can suppose the hydrogen bonding patterns for **1** and **2** are also different (Table 3). Indeed in compound **1** the $B(OH)_2$ moiety participates in a typical O2-H2O…O1 hydrogen bond, producing cyclic dimers with graph set $R_2^2(8)$ (Fig. 4a). The "lateral" interaction of the $B(OH)_2$ group is with another

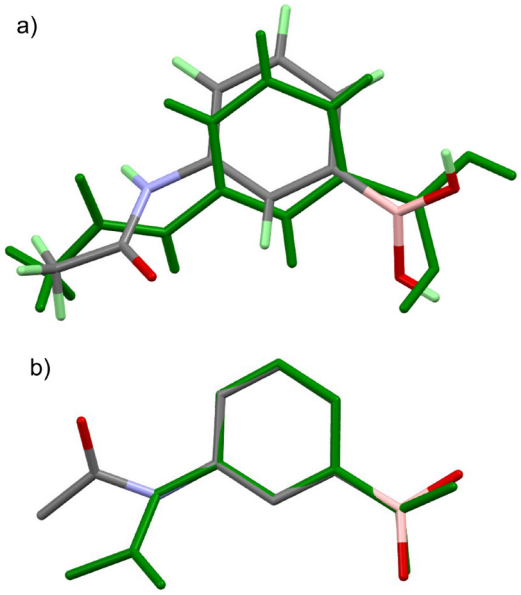

Fig. 3. Overlay of the molecules of **1** (in green) and **2** *a*) superposition of the two independent molecules and *b*) superposition using only the phenyl boronic moiety.

Table 2. Selected distances and bond angles for **1** and **2** (the numbering scheme is as shown on Fig. 3)

Bond distance [Å]			Bond angle [°]			Torsion angle [°]		
	1	**2**		**1**	**2**		**1**	**2**
B1-O1	1.359(4)	1.359(2)	O1-B1-O2	117.8(3)	117.9(2)	O1-B1-C1-C6	23.1(5)	–10.1(3)
B1-O2	1.363(4)	1.361(2)	O1-B1-C1	122.9(3)	118.3(2)	O1-B1-C1-C2	–158.1(3)	170.5(2)
B1-C1	1.561(4)	1.560(3)	C1-C2-C3	121.6(3)	121.6(2)	O2-B1-C1-C6	–155.0(3)	169.2(2)
N1-C3	1.424(4)	1.424(2)	C5-C6-C1	120.8(3)	121.7(2)	O2-B1-C1-C2	23.8(5)	–10.3(3)
N1-C7	1.342(4)	1.344(2)	C3-N1-C7	126.9(2)	127.6(3)	C1-C2-C3-C4	2.1(4)	–0.4(2)
C7-O3	1.226(4)	1.230(2)	N1-C7-O3	123.2(3)	123.2(3)	C3-C4-C5-C6	0.7(5)	1.0(3)
C7-C8	1.497(4)	1.493(3)	N1-C7-C8	115.9(3)	116.5(3)	C2-C3-N1-C7	37.7(5)	157.9(2)
			O3-C7-C8	120.9(3)	120.3(3)	C3-N1-C7-O3	5.1(5)	–5.8(3)

Table 3. Hydrogen bonds (Å, °) in **1** and **2**

D—H···A	D—H	H···A	D···A	< D—H···A
Compound **1**				
N1—H1N···O3^{i}	0.86	2.08	2.925(4)	170
O1—H1O···O2^{ii}	0.81	2.14	2.849(3)	147
O2—H2O···O1^{iii}	0.84	1.93	2.771(3)	175
Symmetry codes: (i) *x, y+1, z*; (ii) *x−1, y, z*; (iii) *−x+1, −y, −z+2*.				
Compound **2**				
N1—H1N···O3^{i}	0.86	2.23	3.069(2)	164
O1—H1O···O2^{ii}	1.09	1.69	2.793(2)	180
O2—H2O···O3^{iii}	0.98	1.78	2.735(2)	162
C4— H4···O3	0.93	2.35	2.882(2)	116
Symmetry codes: (i) *x, −y+1/2, z+1/2*; (ii) *−x+3, −y, −z+2*; (iii) *x+1, −y+1/2, z+1/2*.				

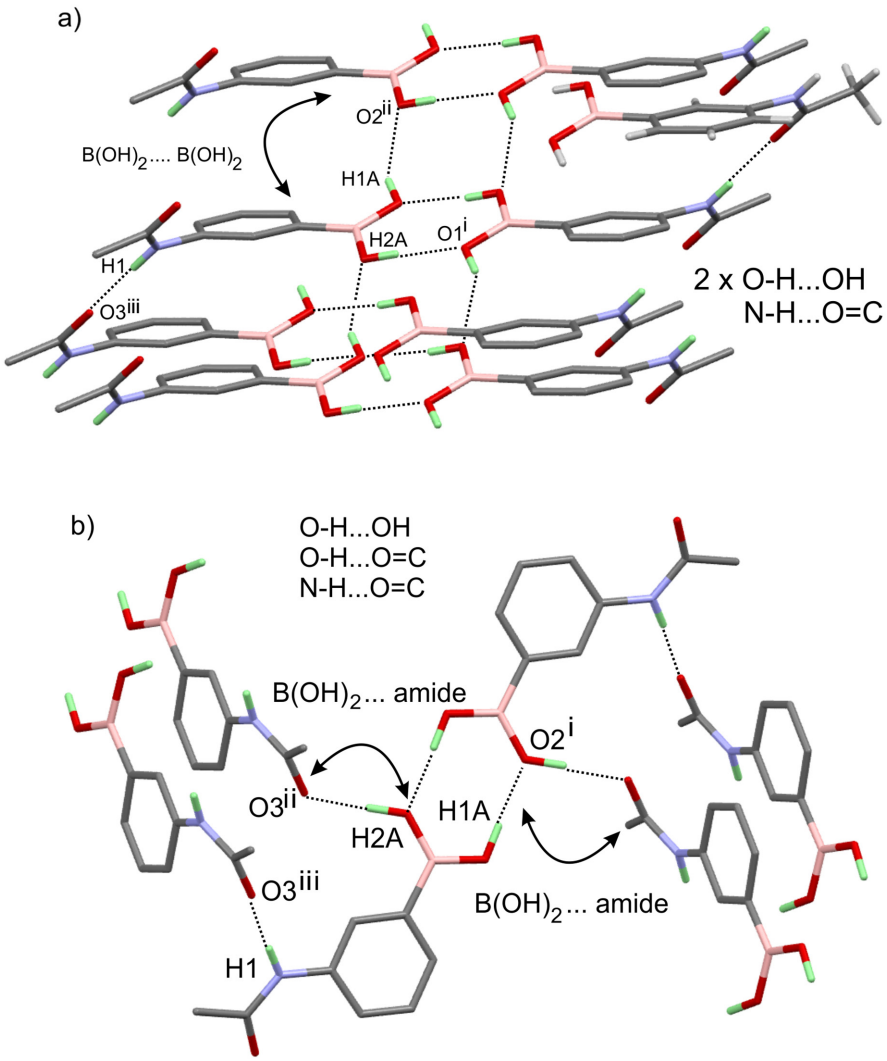

Fig. 4. Hydrogen bonding interactions in *a*) compound **1** and *b*) compound **2**; symmetry operations are listed in Table HB.

$B(OH)_2$, graph set $R_2^2(8)$. The donors and acceptor of the amide fragment are involved in a N1-H1N…O3 hydrogen bond that produces $C_1^1(4)$ chains propagating along *b*. Similarly, in compound **2** an O1-H1O…O2 hydrogen bond (from $B(OH)_2$ moiety) produces cyclic dimers with graph set $R_2^2(8)$. However, the lateral interaction of the $B(OH)_2$ group in 2 is with the amide group O2-H2O…O3 (Fig. 4b). The donors and acceptor of the amide fragment are also involved in an N1-H1N…O3 hydrogen bond $C_1^1(4)$ chains propagating along *c*.

Though in **1** and **2** the hydrogen bonding network is different, the type and number of the hydrogen bonds are the same (two O-H…O and one N-H…O) bonds. This explains the fact that the melting temperatures of two polymorphs are nearly identical.

The *cis* and *trans* isomer geometries were optimized using DFT. Starting geometries were taken from X-ray refinement. The barrier of rotation of the amide group was estimated by calculating the energies resulting from the rotation of the amide moiety along the C3-N1 bond. The *trans* isomer was chosen as a starting point and the potential energy was scanned using a 5° step.

The C-C, B-O, C=O and C-N bond distances and angles characterizing the molecules in the DFT calculated models are comparable to those determined experimentally (Table S1). The observed differences between calculated and observed geometries could e attributed to the crystal packing of the molecules. The DFT calculations showed that the energy difference between the *trans* and *cis* conformers is not considerable (0.9 kcal mol^{-1} in favor of

the *trans* conformer). The computed barrier of rotation of 5.8 kcal mol^{-1} between the two conformers is not excessively high (*cis* to *trans* rearrangement, Fig. 5). However, one should note that the computation does not include the hydrogen bonding interactions present in the crystal and the resulting different orientation of the molecules in the two conformational polymorphs (e.g. in **1** the $B(OH)_2$ group interacts laterally with another $B(OH)_2$ group while in **2** the $B(OH)_2$ group interacts with the amide moiety, Fig. 6). As both moieties (amide and phenyl boronic) are apt to rotate along the C-N bond the synergy leads probably to a lower rotation energy barrier than the one of amide or phenyl groups alone [27, 28]. The conducted *in situ* temperature X-ray powder diffraction experiments showed that Polymorph 1 is converted into polymorph 2 under heating. The conversion start is detected at 135 °C and is completed at 150 °C (Fig. 7). The structure of polymorph 2 is stable up to 270 °C. If the heating is removed and the sample is allowed to cool down slowly to room temperature no phase transition of **2** to **1** is observed (Fig. 8). One should note that the in situ X-ray data does not explain the observed DTA comportment of **2**. One explanation is that the phase transition **2** to **1** is very slow and has not been detected by the *in situ* experiment.

The FTIR spectra of compounds **1** and **2** are illustrated on Fig. 9. Although the crystal system and space group of **1** and **2** are different the spectra show almost identical band positions and intensities. The assignment of the observed bands is as fol-

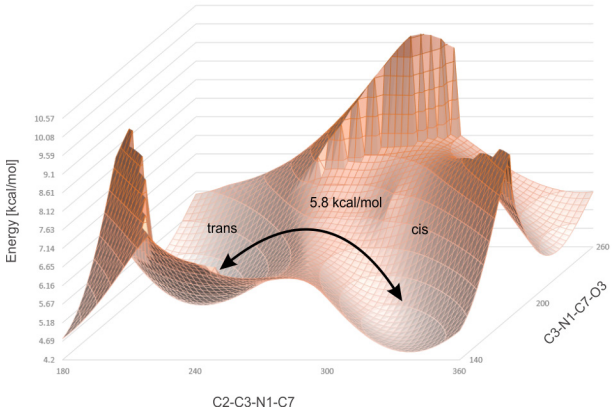

Fig. 5. Potential energy surface and projected contour maps showing the barrier between *trans/cis* conformers (the inset shows the energy surface). The energy corresponds to the difference between single point calculation corresponding to C2-C3-N1-C7 and C3-N1-C7-O3 angles and the global minimum energy, with a positive offset of 4 kcal.

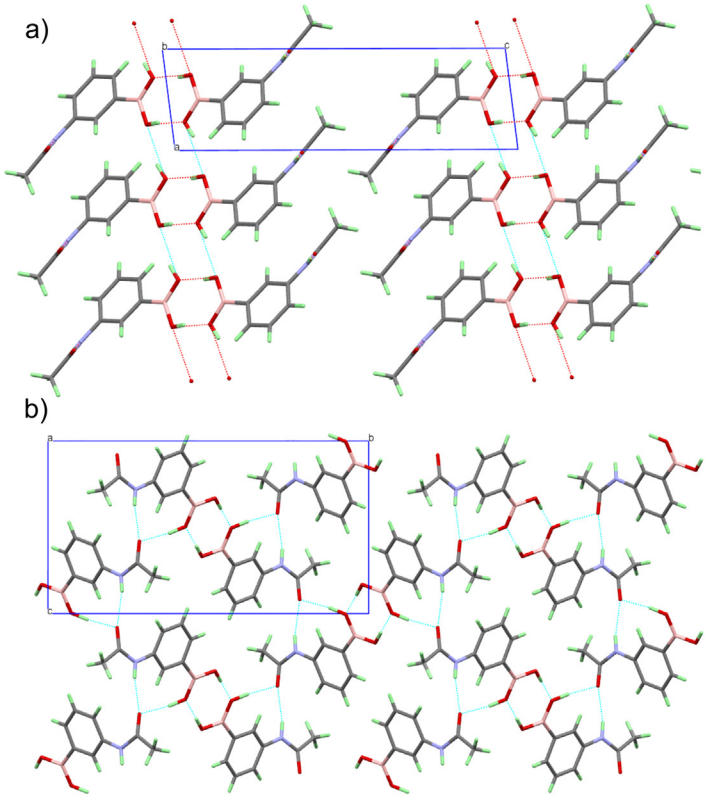

Fig. 6. Three-dimensional arrangement of the molecules in a) compound **1** and b) compound **2.**

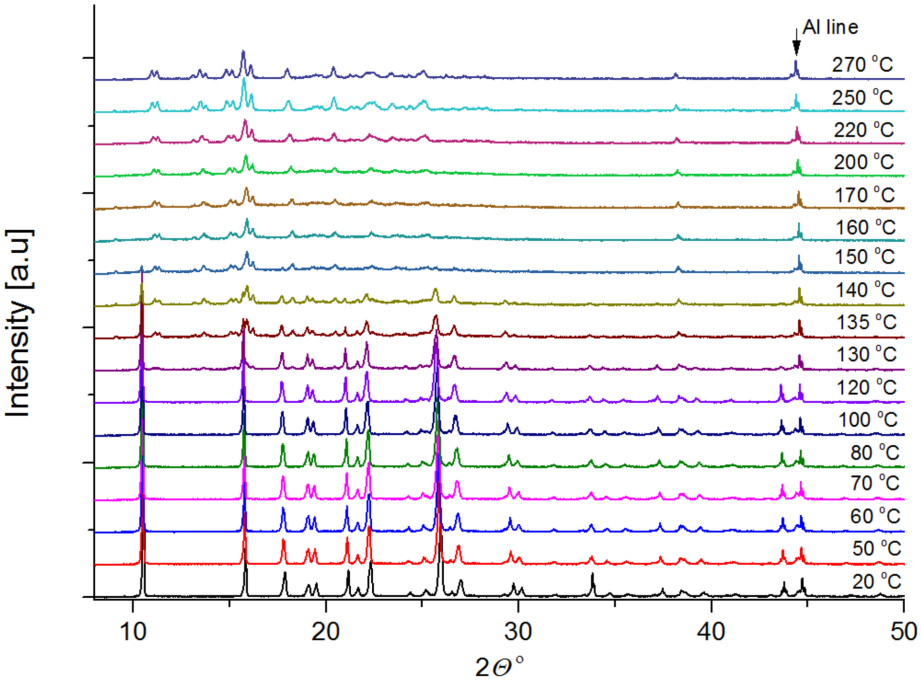

Fig. 7. *In situ* temperature X-ray powder diffraction experiments starting with polymorph1.

lows: the bands at $\gamma_{(s)}$526 cm^{-1}a and $\delta_{(s)}$593 are associated to bending O-H vibrations while the band at $\gamma_{(as)}$650 cm^{-1} is related to B-O from –B(OH)$_2$ group. The peak at 1118 cm^{-1} is due to the νB-C vibration mode. In the range 1200 to 1460 cm^{-1} several overlapping bands with maxima at 1424, 1348, 1295 and 1220 cm^{-1} are observed. They can be related to $\nu_{(as)}$B-O, νC-C (in ring), δC-H (or rocking) and νC-N vibrations [29]. The bands at 1542 and 158 5cm^{-1} are connected with aromatic group δC–C and $\delta_{(rock)}$ NH vibrations while the band at 1660 cm^{-1} belongs to C=O. The asymmetric and symmetric stretches of methyl group appear at $\nu_{(as)}$2839 and $\nu_{(s)}$2988 cm^{-1} [30] respectively. The weak band at 3074 cm^{-1} is associated to the νC–H vibration. The strong band at 3309 cm^{-1} is related to νO-H and strong hydrogen bonding while the band at 3430 cm^{-1} (with medium intensity) corresponds to N–H stretch.

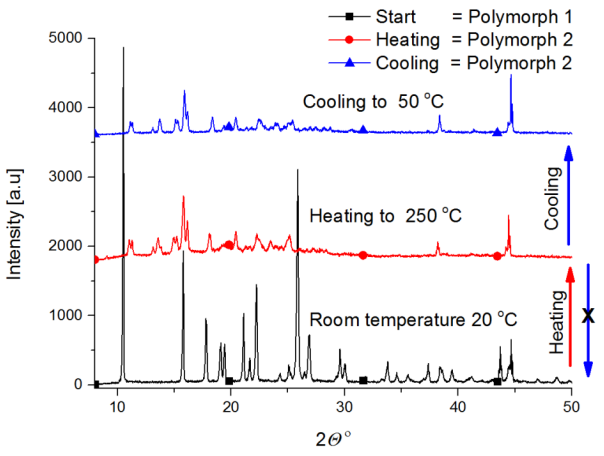

Fig. 8. Observed phase transitions of **1** and **2** with temperature: heating to 270 °C and the slow cooling to room temperature.

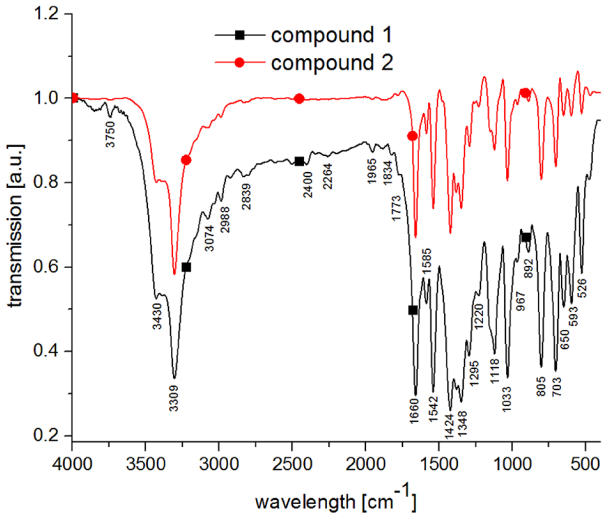

Fig. 9. FTIR spectra of compound **1** and **2**.

CONCLUSIONS

Two conformational polymorphs of (3-acetamidophenyl)boronic acid were obtained and characterized by single crystal diffraction analyses, FTIR and DFT to further elucidate the crystal formation mechanisms. The two polymorphs exhibited almost identical thermal and spectral absorption features (in the range 400–4000 cm^{-1}). This result is further supported by DFT calculations showing minimal energy difference between the two conformers (molecules). The crystal structures solution pointed that the hydrogen-bonding scheme was different in the two polymorphs, while the type and number of interactions remained the same. The same number of hydrogen bonding interactions present in both polymorphs is probably the main reason for the observed almost identical thermal comportment of the modifications. The results suggest that in order to correctly describe and identify different crystalline polymorphic forms the combination of employed methods must include diffraction experiments.

Acknowledgments: *This work was supported by NSF Grant DRNF 02/1 and T02/14.*

REFERENCES

1. C. Y. Liu, Y. Li, J. Y. Ding, D. W. Dong, F. S. Han, *Chem-Eur. J.*, **20**, 2373 (2014).
2. T. Moriya, N. Miyaura, A. Suzuki, *Chem. Lett*., **22**, 1429 (1993).
3. S. I. Miyatake, M. Furuse, S. Kawabata, T. Maruyama, T. Kumabe, T. Kuroiwa, K. Ono, *Neuro-Oncology*, **15,** 650 (2013).
4. R. Asano, A. Nagami, Y. Fukumoto, K. Miura, F. Yazama, H. Ito, I. Sakata, A. Tai, *Bioorg. Med. Chem. Lett.*, **24,** 1339 (2014).
5. J. K. Zhang, L. Q. Shen, J. C. Wang, P. H. Luo, Y. Z. Hu, *Med. Chem*., **10,** 38 (2014).
6. J. Wang, W. Wu, Y. J. Zhang, X. Wang, H. Q. Qian, B. R. Liu, X. Q. Jiang, *Biomaterials*, **35**, 866 (2014).
7. Z. F. Xu, K. M. A. Uddin, T. Kamra, J. Schnadt, L. Ye, *Appl. Mater. Inter*., **6**, 1406 (2014).
8. M. Kumai, S. Kozuka, M. Samizo, T. Hashimoto, I. Suzuki, T. Hayashita, *Anal. Sci*., **28**, 121 (2012).
9. W. Takayoshi, M. Imajo, M. Iijima, M. Suzuki, H. Yamamoto, Y. Kanekiyo, *Sensor Actuat. B-Chem*., **192**, 776 (2014).
10. V. V. Zhdankin, P. J. Persichini, L. Zhang, S. Fix, P. Kiprof, *Tetrahedron Lett*., **40**, 6705 (1999).
11. J. H. Fournier, T. Maris, J. D. Wuest, W. Z. Guo, E. Galoppini, *J. Am. Chem. Soc*., **125**, 1002 (2003).
12. E. R. T. Tiekink, J. J. Vittal, M. Zaworotko, *Organic crystal engineering: frontiers in crystal engineering, Wiley, Chichester, U.K*., 2010.
13. H. G. Brittain, *Polymorphism in pharmaceutical solids, 2nd ed., Informa Healthcare*, New York, 2009.
14. G. R. Desiraju, *Crystal design: structure and function*, Wiley, Chichester, West Sussex, England; Hoboken, NJ, 2003.
15. J. Elguero, *Cryst. Growth Des*., **11**, 4731 (2011).
16. A. Nangia, *Accounts Chem. Res*., **41**, 595 (2008).
17. CAD-4 EXPRESS. Version 5.1/1.2. Enraf Nonius, Delft, the Netherlands.
18. Agilent, in, Agilent Technologies, UK Ltd, Yarnton, England, 2011.
19. G. M. Sheldrick, *Acta Crystallogr*. A, **64**, 112 (2008).
20. L. Farrugia, *J. Appl. Crystallogr*., **30**, 565 (1997).
21. C. F. Macrae, I. J. Bruno, J. A. Chisholm, P. R. Edgington, P. McCabe, E. Pidcock, L. Rodriguez-Monge, R. Taylor, J. van de Streek, P.A. Wood, *J. Appl. Crystallogr.*, **41**, 466 (2008).
22. M. J. Frisch, G. W. Trucks, H. B. Schlegel, G. E. Scuseria, M. A. Robb, J. R. Cheeseman, G. Scalmani, V. Barone, B. Mennucci, G. A. Petersson, H. Nakatsuji, M. Caricato, X. Li, H. P. Hratchian, A. F. Izmaylov, J. Bloino, G. Zheng, J. L. Sonnenberg, M. Hada, M. Ehara, K. Toyota, R. Fukuda, J. Hasegawa, M. Ishida, T. Nakajima, Y. Honda, O. Kitao, H. Nakai, T. Vreven, Jr, J. E. Peralta, F. Ogliaro, M. Bearpark, J. J. Heyd, E. Brothers, K. N. Kudin, V. N. Staroverov, R. Kobayashi, J. Normand, K. Raghavachari, A. Rendell, J. C. Burant, S. S. Iyengar, J. Tomasi, M. Cossi, N. Rega, J. M. Millam, M. Klene, J. E. Knox, J. B. Cross, V. Bakken, C. Adamo, J. Jaramillo, R. Gomperts, R.E. Stratmann, O. Yazyev, A.J. Austin, R. Cammi, C. Pomelli, J. W. Ochterski, R. L. Martin, K. Morokuma, V. G. Zakrzewski, G. A. Voth, P. Salvador, J. J. Dannenberg, S. Dapprich, A. D. Daniels, Farkas, J. B. Foresman, J. V. Ortiz, J. Cioslowski, D. J. Fox, Gaussian 09 Revision A.02, Gaussian Inc. Wallingford CT 2009, 2009.
23. C. Lee, W. Yang, R. G. Parr, *Phys. Rev*. B, **37**, 785 (1988).
24. A. D. Becke, *J. Chem Phys*., **98**, 5648 (1993).
25. V. Dyulgerov, R. P. Nikolova, L. T. Dimova, B. L. Shivachev, *Acta crystallogr*. E., **68**, o2320 (2012).
26. D. Zhang, L. E. Harrington, H. Tanaka, R. Pelton, *Acta Crystallogr*. E, **63**, o4628 (2007).
27. R. Chaudret, G. Trinquier, R. Poteau, L. Maron, *New J Chem*., **33**, 1833 (2009).
28. V. S. Dimitrov, V. B. Kurteva, M. J. Lyapova, B. P. Mikhova, I. G. Pojarlieff, *Magn. Reson. Chem*., **26**, 564 (1988).
29. J. A. Faniran, H. F. Shurvell, *Can. J. Chem*., **46**, 2089 (1968).
30. M. Avram, G. D. Mateescu, Infrared spectroscopy: applications in organic chemistry, Wiley-Interscience, New York, 1972.